VOL. 15, NO. 11, JUNE 2020 ISSN 1819-6608
ARPN Journal of Engineering and Applied Sciences
©2006-2020 Asian Research Publishing Network (ARPN). All rights reserved.
www.arpnjournals.com

INFLUENCE OF ABRASIVE WHEELS CHARACTERISTICS ON PHASES CHANGE OF NITINOL IN DIFFERENT STRUCTURAL CONDITIONS

Soler Y. I. and Kazimirov D. Yu.
Department of Mechanical Engineering Production Technologies and Equipment, Irkutsk National Research Technical University, Lermontova St., Irkutsk, Russian Federation
E-Mail: solera@istu.irk.ru

ABSTRACT

The aim of this work is to evaluate changes of nitinol structure in the condition of austenite and martensite during grinding of surfaces. Different abrasive wheels and constant grinding mode were used in the experiment. The composition of nitinol was studied by x-ray phase analysis. It was found that the grinding of nitinol, when it is in austenite state better retains phase fraction than in martensite state. Grinding leads to secondary intermetallic compounds formation, as well as basic phases decrease as compared with the parent state. Abrasive wheel characteristics have a noticeable but not unambiguous effect on the stability of the phases. NiTi phases' content boundaries, as well as their absolute change after grinding have been determined.

Keywords: grinding, nitinol, phases, X-Ray.

INTRODUCTION

Shape memory effect (SME) alloys are widely used in aerospace, oil and gas, medical and other industries [1]. The TN-1 alloy (titanium nickelide or nitinol) is the main among materials with SME by the degree of physical research and application. In Russia, there is a lag of several years from the advanced countries in the development of technologies and production of shape memory alloys, despite the need for their wide application in these industries. Production of nitinol in Russia does not exceed 1 and 15 % of its production in the US and China, respectively. Currently, the work on the strategic development of Russia in this direction is being intensified [2].

Nitinol and double TiNi-based alloys have valuable mechanical and physical-chemical properties, for example, thermal shape memory, superelasticity, biocompatibility, cavitation resistance and the ability to dampen vibrations in the audio frequency range [3, 4]. In connection with motioned above, they are used as functional and structural materials.

Studies [5, 6] confirmed their high fatigue strength, wear resistance (abrasive and adhesive components), as well as good corrosion resistance [7], especially in aggressive environments.

It is known that nitinol and other titanium-based intermetallics have low machinability with edge tools [8, 9, 14], therefore grinding [11-13], burnisning, polishing and lapping, EDM machining are used for them [14], and also combined edge machining processes [10], where titanium nickelide shows increased machinability. Fine-grained structure of TN-1 alloy leads to increasing machinability during machining, tensile strength and microhardness of the surface. The result of successful grinding application is the property of the surface to suppress the grooves formation during micro-cutting [6]. The movement of the abrasive grain proceeds without formation of stress concentrators on the parts. However, grinding affects the reduction of corrosion resistance, which is increased by subsequent electropolishing. It is possible to use SME alloy with coarse-grained structure TiNi-Fe, because after grinding it is more resistant to corrosion than Ti-Ni of a similar structure.

From a practical point of view, the following functional properties of TN-1 alloys with SME are of interest: reversible deformation consisting in the ability to accumulate deformation during cooling in the absence of loading. The parent B2-austenite lattice is transformed into a monoclinic B19-martensite lattice (see Figure-1). When heated, the alloy is able to return relatively large deformations. There is also a phenomenon of pseudoelasticity, in which plastic deformation is restored after taking of the load off.

TN-1 alloy can be in two structural states: low-temperature, called «martensite», and high-temperature - «austenite». The characteristic of «martensite» structure in SME alloy is fundamentally different from the concept of steel martensite in which it has high hardness and brittleness. On the contrary, martensite of this material is characterized by high plasticity and well deformability, and austenite in SME alloys is more rigid and durable.

By susceptibility to heat effect all Ti-Ni-based alloys can be divided into two groups. The first group includes compositions with 49.5-50.5% Ni, in which there is no diffusional decay of the B2-phase. The second group includes alloys containing more than 50.5% atomic (at. %) Ni, where B2-phase can be undergoes multistage diffusional decay. Structural analysis of titanium nickelide was investigated in [16]; in which phase transformations (Figure-1) at the time of the martensitic transformation when heated to temperatures close to the values during grinding and air cooling were established. However, there are no studies of structural-phase compositions after grinding of titanium nickelide. Since this alloy does not have constant points of martensite transformation (MT), obtaining a reversible SME implies the need for a clear control of the stability and degradation effects due to material processing technology.

©2006-2020 Asian Research Publishing Network (ARPN). All rights reserved.

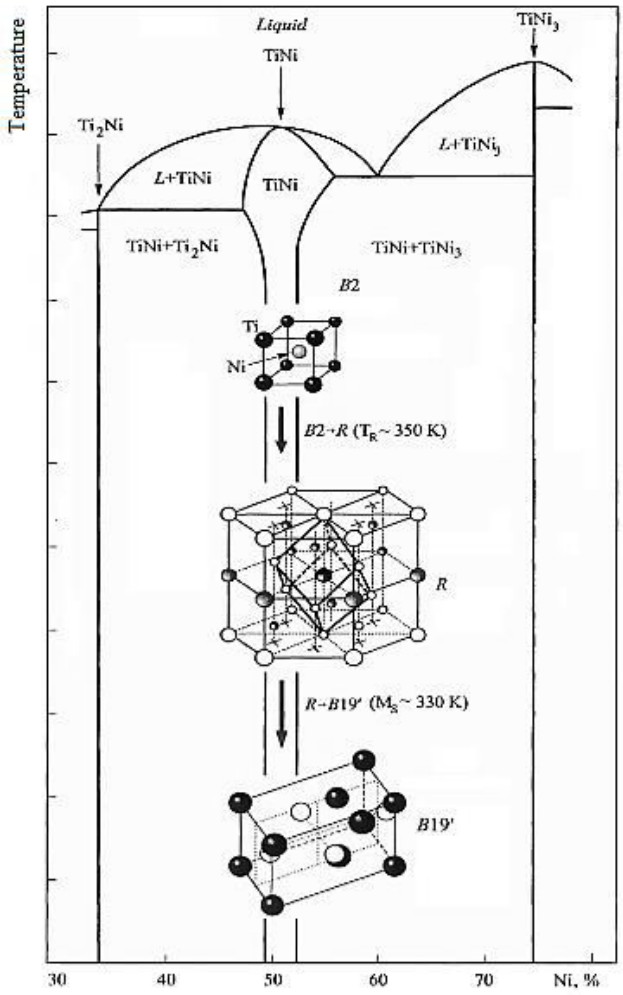

Figure-1. Phase diagram and crystal structures of titanium nickelide [21].

MATERIALS AND METHODS

The object of study - samples of TN-1 alloy of the following composition: $Ti_{45.04}Ni_{54.96}$ - A and $Ti_{44.31}Ni_{55.69}$ - B (at. %), (Russian production, L.L.C. «Matek-SPF», Moscow). The option A - as-received condition alloy, the option B - the alloy subjected to hardening at 673 K in water, that give the temperature of the reverse martensitic transformation Af=351 and 298 K, respectively. In the coarse-grained state the alloy has a tensile strength $\sigma_B \approx 800...900$ MPa. In the austenite state, microhardness of alloy is Hμ=4050 MPa, and in the martensite state - Hμ=3500 MPa. All studies were conducted at room temperature on the X-ray diffractometer Shimadzu XRD-7000 in the center for collective use «Baikal center of nanotechnology» (Irkutsk, Russia) using Cu-Ka radiation with a wavelength of 1.541874 A^o in 2θ angle range from 10.0° to 80.0°.

RESULTS AND DISCUSSIONS

Phase composition of TN-1 alloy in the parent state

According to the micro-diffraction pattern and X-ray diffraction analysis, the TN-1B material after pressing and heat treatment is represented by a basis of austenitic B2-phase of titanium nickelide; and the martensitic B19' phase with a monoclinic crystal lattice is not detected. Wide peaks (Figure-2) of material main phase on the X-ray diagrams indicate a coarse-grained crystal structure. Oxides in the form of interstitial impurity with a complex crystal lattice also present in titanium nickelide. As is known, titanium oxide formation, such as TiO_2, has a protective effect, but it worsens the mechanical properties, reduces the ability to deformation, and in the formation of complex oxides - reduces its plasticity. At low temperatures in TiO-system TiO_2, and also Magnely phases, which are represented by discrete compounds of the homologous series Ti_nO_{2n-1} ($10 \geq n \geq 4$): Ti_3O_5, Ti_2O_3, TiO, Ti_2O, Ti_3O and Ti_6O, precipitate.

©2006-2020 Asian Research Publishing Network (ARPN). All rights reserved.

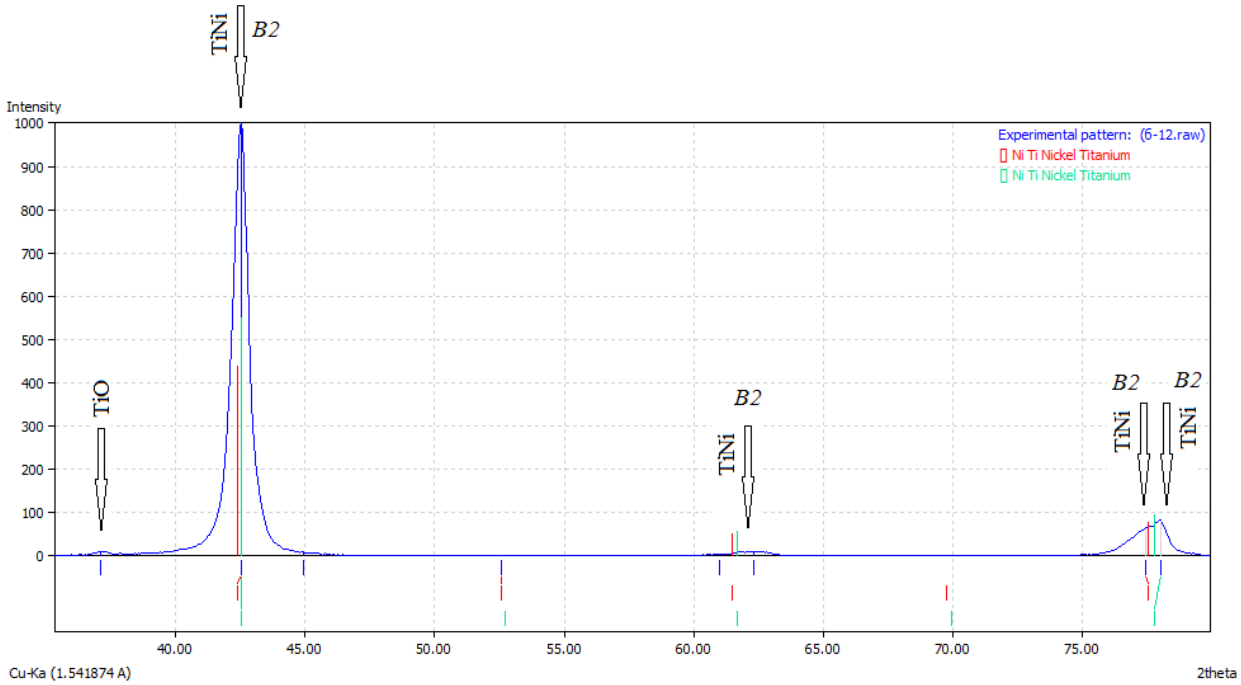

Figure-2. X-ray diagram of the TN-1B alloy phase composition in the parent state.

A more complex phase composition takes place for the TN-1A alloy (Figure-3). The presence of martensitic B19' phase in the amount of 17.6% is noted, that is consistent with the generally accepted concepts of alloys with high temperature MT. The largest volume ratio also belongs to the austenitic B2 phase, as evidenced by the intensity of peaks for 2θ≈43, 62 and 73^0. The presence of titanium oxide in a small volume fraction (6.5%) completes the diffraction pattern of nitinol in as-received condition. In general, it can be noted that the phase state which was evaluated by the X-ray diffractometer Shimadzu with an exposure time of 12 hours, is gone with the literature data.

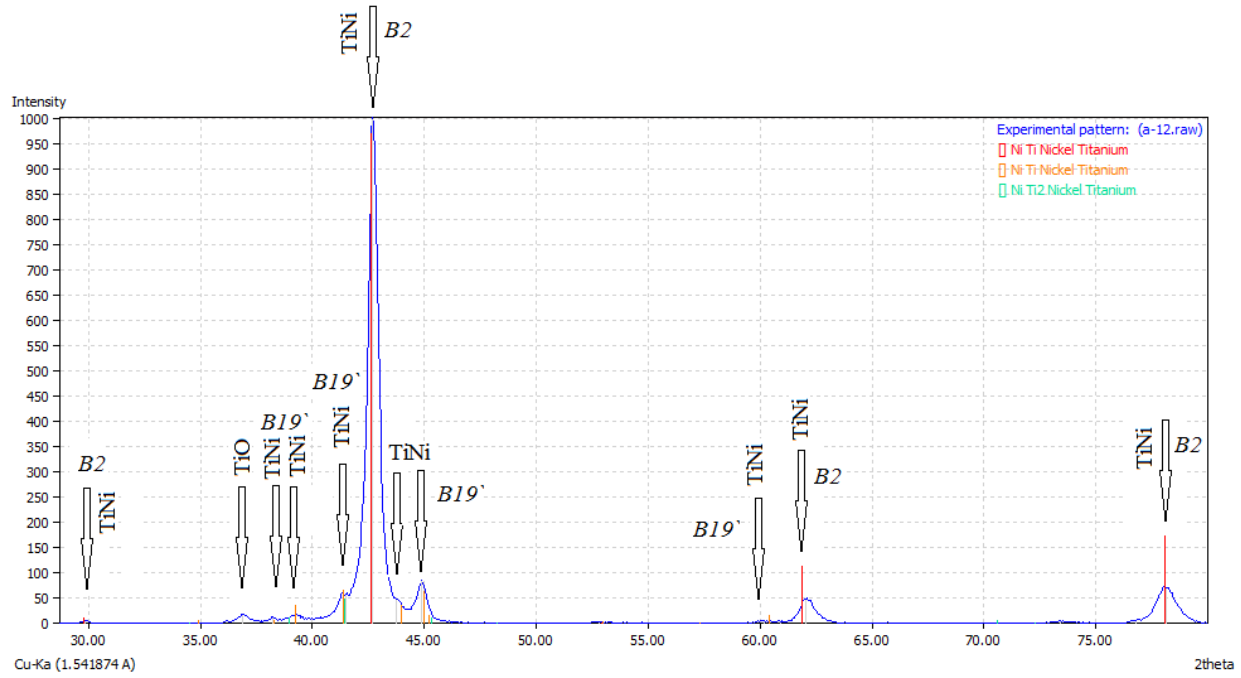

Figure-3. X-ray diagram of the TN-1A alloy phase composition in the parent state.

©2006-2020 Asian Research Publishing Network (ARPN). All rights reserved.

The titanium nickelide alloy at room temperature is in the martensitic phase with a double monoclinic crystal lattice adequate to «normal conditions» (Figure-4). The force action of the processing tool can lead to a non-twinned monoclinic crystal lattice. In this case, the external form will remain prismatic - a detwinning takes place. When heated, a phase transition to an austenitic cubic crystal lattice occurs. Upon cooling the form returns to the monoclinic structure [18].

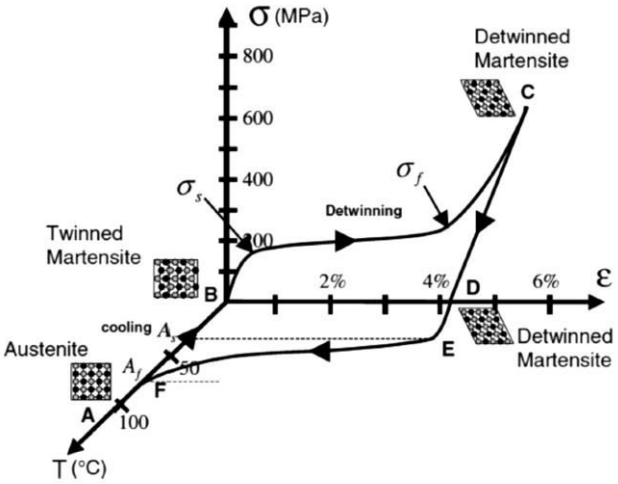

Figure-4. Graph of the relationship «stress-deformation-temperature» for ordinary alloy NiTi [8].

It is known that reversible SME in titanium nickelide is correlated with volume ratio of phases: B2, which is reflecting mechanical properties and B19` - martensitic transformation. Therefore, qualitative and quantitative analysis of changes after the widespread method of forming and surface quality engineering known as grinding - was carried out.

Samples with dimensions D×H = 40×35 mm were face-processed on a flat-grinding machine model 3G71; flooded coolant - 5% emulsion Aquol–6 at rate of 7-10 l/min. The shapes and characteristics of the abrasive wheels are shown in Table-1. Grinding mode: wheel speed v_w = 35 m/s, longitudinal feed s_l = 6 m/min; cutting depth t = 0.01 mm; transverse feed s_t = 4 mm/double stroke, allowance z =0.1 mm.

Table-1. Used abrasive tools.

Code	Shapes and size	Wheel characteristics
i=1	01 250x25x76 *(Molemab, Italy)*	08C 070 I12 V01 P1
i=2	01 250x25x76 *(Molemab, Italy)*	08C 046 I12 V01 P1
i=3	1 250x20x76 (Volzhsky Abrasive Works, Russia)	63C F46 L7V

Wheels i = 1, ..., 3 are made of silicon carbide green. Grain grades (08C, 63C), abrasive grit, hardness, structure and porosity were varied in the wheels.

Grinding by 08 C070 I12V01P1 wheel

Analysis of the sample surface diffractogram of alloy TN-1B grinded by wheel i=1, showed the following change in compared to the parent state. The crystal lattice has undergone stretching, which is seen from the left-shifted peak of the B2-phase for $2\theta \approx 67^0$. The austenite phase of titanium nickelide with a cubic lattice exceeded the volume ratio that is clearly seen in Figure-5 by peak intensity for $2\theta \approx 62^0$, which has I≈190 c. u. (conditional unit) after grinding at initial one of 90 c. u. The peaks belonging to the phase with monoclinic crystal lattice TiNi ($2\theta \approx 45^0$) and intermetallic, which was recognized as NiTi2 ($2\theta \approx 40^0$), are also obtained. However, the number of this phase is necessary to additionally determine due to low pick's intensity. After grinding, the parent oxide film of complex molecular formula was removed (in Figure-5, it is simplified as TiO).

©2006-2020 Asian Research Publishing Network (ARPN). All rights reserved.

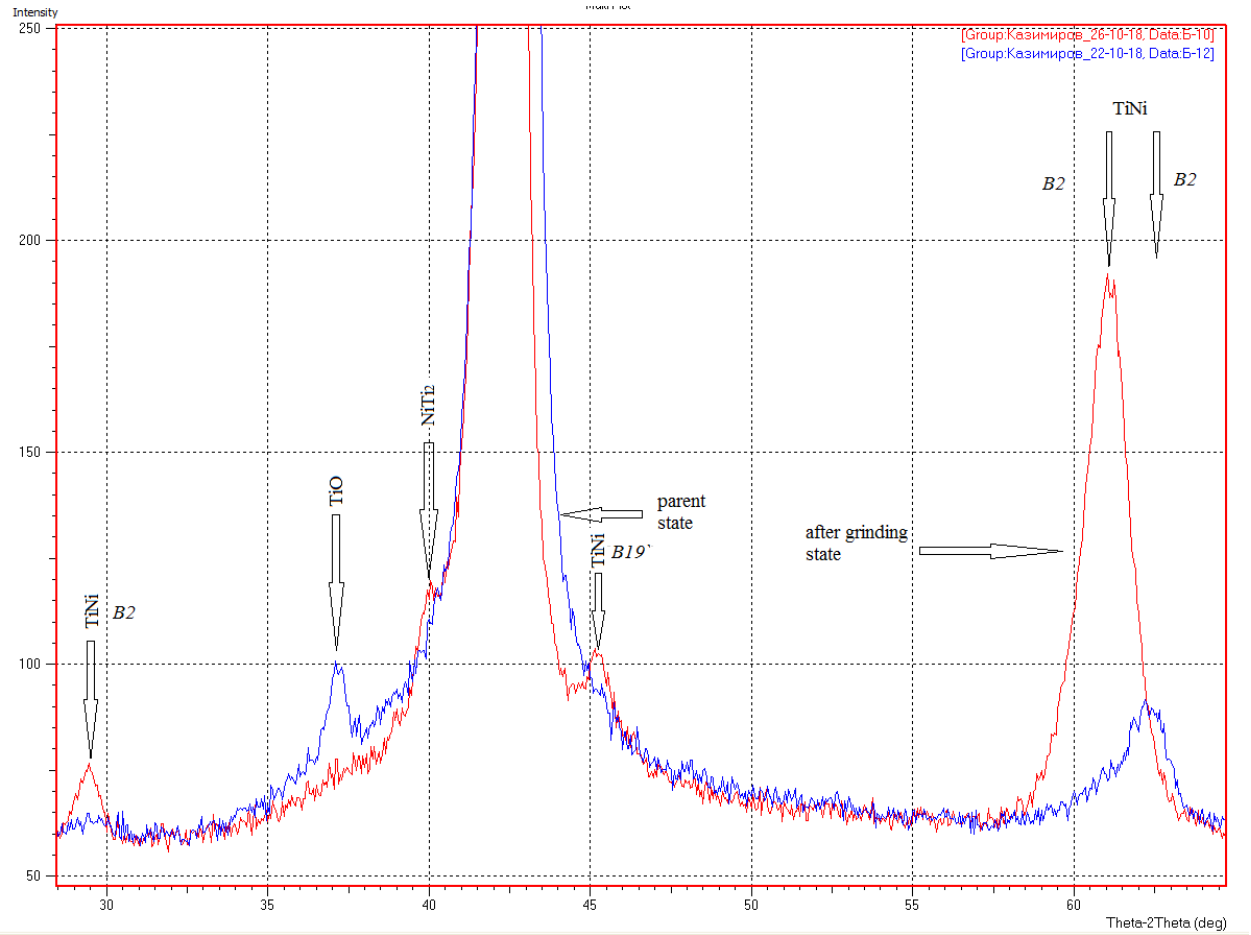

Figure-5. X-ray diagram of the TN-1B alloy phase composition in the parent state and after grinding by wheel *i*=1.

It is known that the high mechanical properties of TiNi alloys depend on the ability of Ni-Ti matrix to experience martensitic transformation B2-B19', and the absence of brittle phases in the bundle. At the same time, the maximum strength properties are demonstrated by the alloy with the highest content of B2-phase titanium nickelide. For this reason, it is necessary to clarify the lower confidence limit of austenitic phase volume ratio, for this purpose, an additional study for two similarly machined samples was performed.

According to the RiR-method (relative intensity ratio method) data on the possible composition of the TN-1B examined phases were obtained, which are summarized in Table-2.

Table-2. Volume fraction of phases in grinded samples TN-1B.

Phase	Phase fraction, %				
	Samples			Results	
	9	10	11	Average	Standard deviation
NiTi B2-phase	80.6	82.4	94.4	85.80	7.50
NiTi B19`-phase	7.1	6.9	3.5	5.83	2.02
$NiTi_2$	12.3	10.7	2.1	8.37	5.49

The results were tested using Student's criterion for small sample. It was predicted that the lower limit of austenitic phase volume fraction is characterized by the interval estimate of the average (85.80 -12.7)% at $t_{0.95}$=2.92.

Nickel and titanium form a number of stable chemical compounds: $NiTi_2$, Ni_3Ti. In this case, intermetallic $NiTi_2$ has a complex cubic lattice. Grinding of bars with this tool under the influence of cutting force and heat flow led to the separation of $NiTi_2$ intermetallic compounds characteristic of the alloy. Figure-6 shows the X-ray diffraction spectrum with the presence of B2 and B19` titanium nickelide phases. At the same time, a brittle negative intermetallic phase was detected at $2\theta \approx 40^0$. In fact, this courses to reduce of alloy plasticity and increases the risk of parts destruction during operation (in service)

©2006-2020 Asian Research Publishing Network (ARPN). All rights reserved.

[17]. As can be seen from Table-2, the sample № 9 has the largest ratio of considered intermetallic equal to 12.3%, and the smallest fraction of strength B2-phase titanium nickelide – 80.6%.

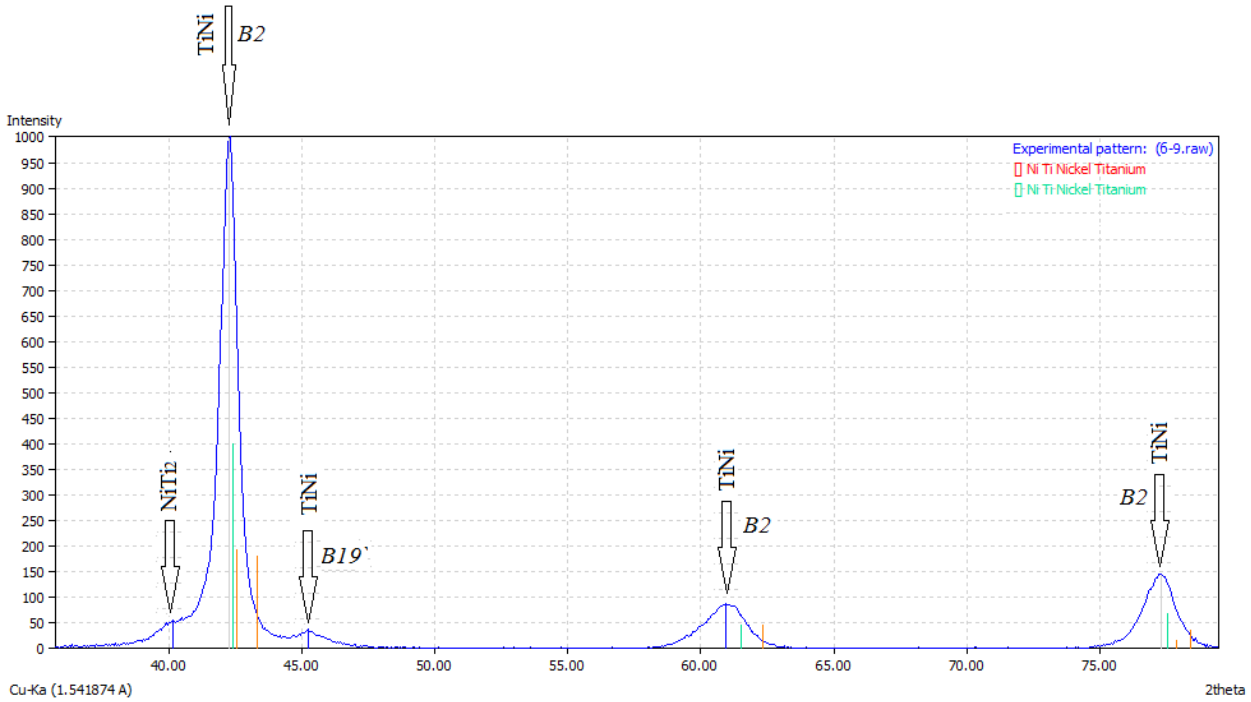

Figure-6. X-ray diagram of TN-1B alloy phase composition (sample № 9) after grinding by wheel *i*=1.

On sample № 11 (Figure-7) during the RiR-method it was determined that the number of non-basic intermetallic phases is below the level of reliability of 5%, which can be neglected. The standard deviation of the content calculated for this phase of 5.49% makes it unlikely that there is a brittle phase, as the lower limit is defined as insignificant. The material is mainly represented by austenite with the highest peak intensity among the compared samples and a relative content of 94.4%.

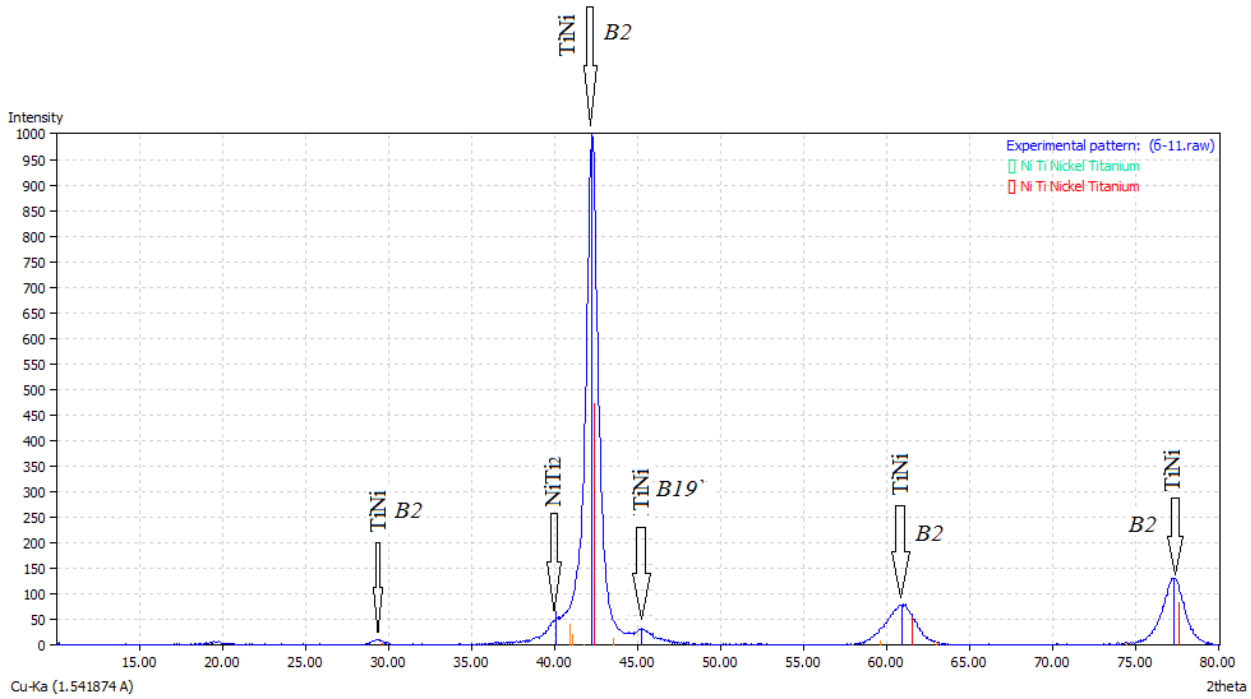

Figure-7. X-ray diagram of the TN-1B alloy (sample № 11) after grinding by wheel *i*=1.

©2006-2020 Asian Research Publishing Network (ARPN). All rights reserved.

For the material TN-1A treated with a circle *i*=1, the following characteristics of the structure are observed. As in the previous case, the crystal lattice is in a deformed state with a characteristic peak distortion in the form of a shift to $2\theta \rightarrow 0^0$. B2-phase cubic crystal lattice state changed in comparison with the parent state due to the decrease in the intensity of the peaks from I≈2200 to 1300 c. u. at $2\theta \approx 43^0$ (Figure-8). This indicates its degradation, decay, including a quantitative decrease in concentration. The martensite structure with a monoclinic crystal lattice was partially restored as a result of the temperature and force effect of the grinding tool. The oxide film is removed from the surface when removing the operating allowance z=0.1 mm by grinding.

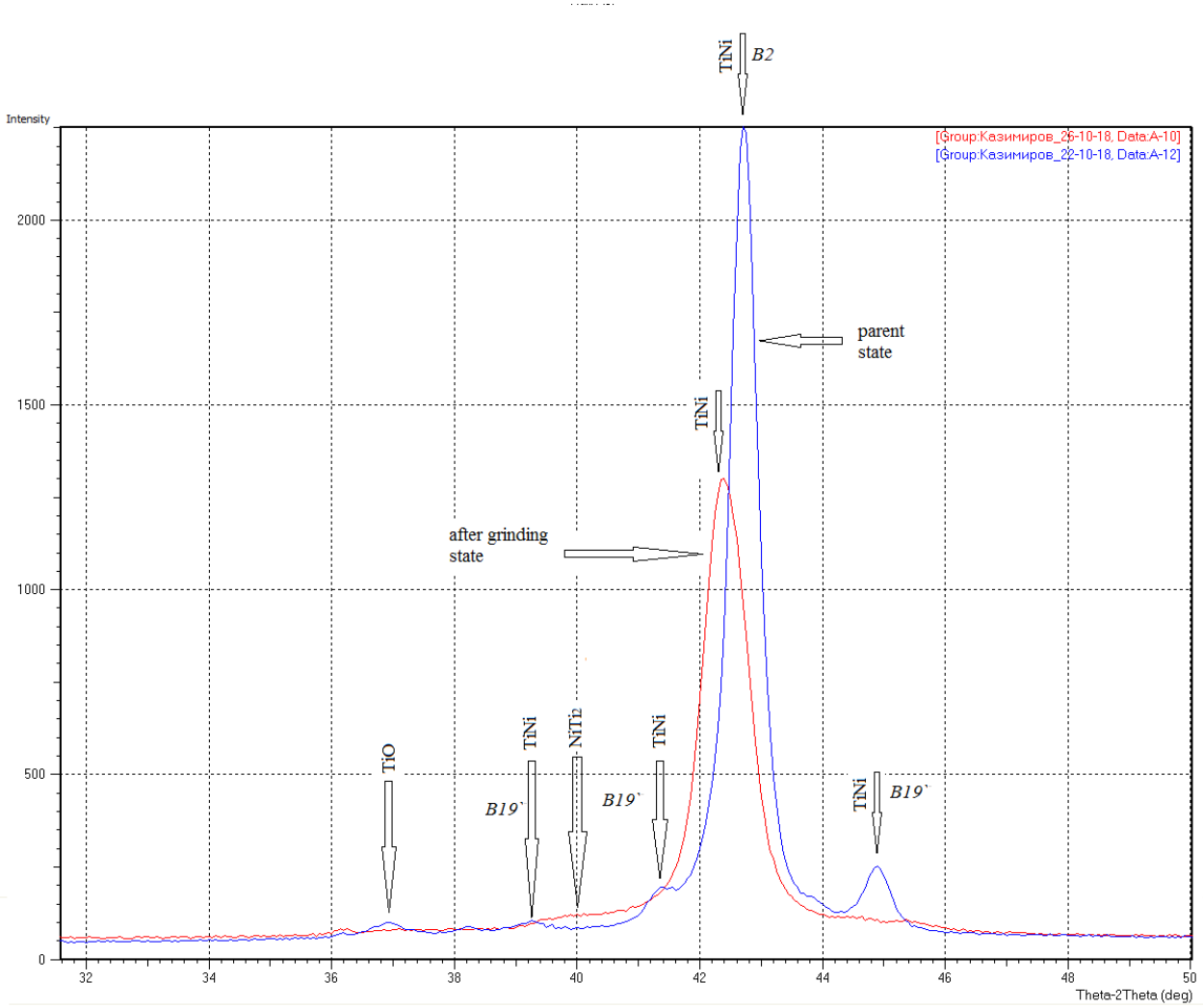

Figure-8. X-ray diagram of the TN-1A alloy phase composition in the parent state and after grinding by wheel *i*=1.

As mentioned earlier, the alloy strength properties depend on the microstructure and phase composition of the alloy. It is not reliably established, but intermetallic $NiTi_2$, as well as for TN-1B, is determined by the intensity I=50 c. u. at $2\theta \approx 40^0$. The reference for this compound has another characteristic pick of intensity, which in our case is absent in the diffraction pattern. Due to the fact that the content of $NiTi_2$ is insignificant, negative changes in the product because of intermetallic after grinding are unlikely, but they quite possible due to alloy non-return to its parent structural state.

Grinding by wheel 08 C046 I12V01P1

After grinding of TN-1A sample it retains the parent phase composition, but changes in XRD pattern is also clearly visible. As shown in Figure-9 austenite B2-phase is decreased, since the intensity of the peak decreased in two times from I=2250 to 1250 c. u. at $2\theta \approx 43^0$ and less - at $2\theta \approx 62^0$. There is an undesirable decrease in martensite phase fraction as compared to the parent one, since the peak characteristic for the fraction at $2\theta \approx 45^0$ has lost from 250 to 100 c. u. in its intensity I. This leads to a shift at the point of reverse MT in recycles of B2-B19`transformation. The active titanium oxides (on Figure-9 they are indicated as TiO) largely remained at the same level. It was noted that the Ni_3Ti fine phase precipitated in an amount at the confidence limit of 5%. Precipitation of secondary phases can lead to a variation in austenite composition, which will cause a change in MT temperature. It is known that in intermetallic TiNi-based

©2006-2020 Asian Research Publishing Network (ARPN). All rights reserved.

alloys, the critical points of martensite transformations are very sensitive to thermomechanical effects [1]. As mentioned earlier it is undesirable to allow significant changes in the B2-phase.

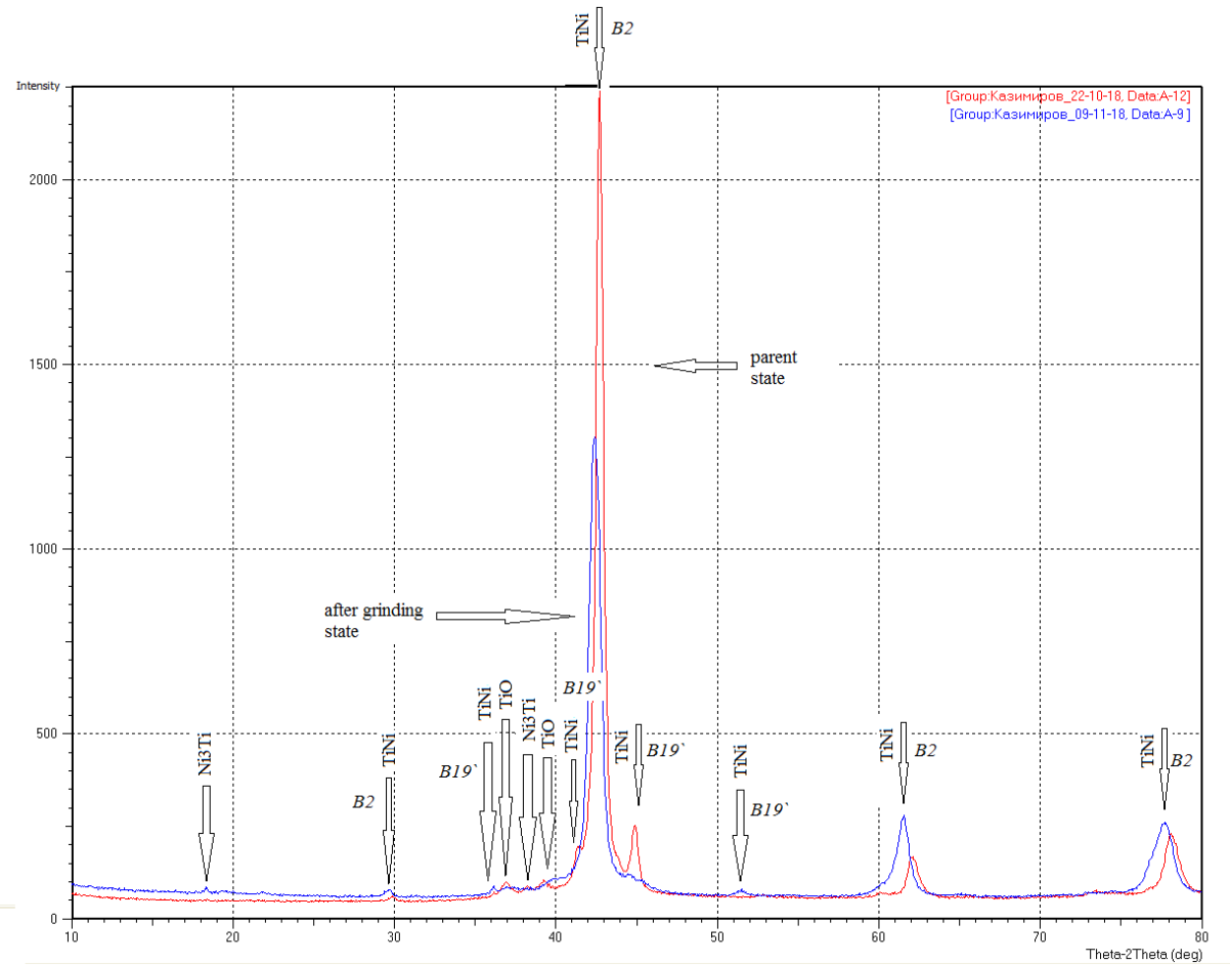

Figure-9. X-ray diagram of TN-1A alloy phase composition in the parent state and after grinding by wheel *i*=2.

To obtain averaged relative phase composition, the X-ray diffraction analysis was duplicated for another TN-1A prototype sample under identical conditions. Although it was a palliative, however, it is associated with the high cost and duration of such measurements, especially for metals with a close-packed crystal lattice. As shown in Figure-10, the pattern is similar, especially in terms of phase qualitative composition of titanium nickelide with monoclinic and cubic crystal lattices. The difference has been noted only in the content of active titanium oxides. The results of the RiR method with the possible ratios of the TN-1A studied phases are summarized in Table-3. It also provides a comparison of peak intensities that indicates structural transformations.

©2006-2020 Asian Research Publishing Network (ARPN). All rights reserved.

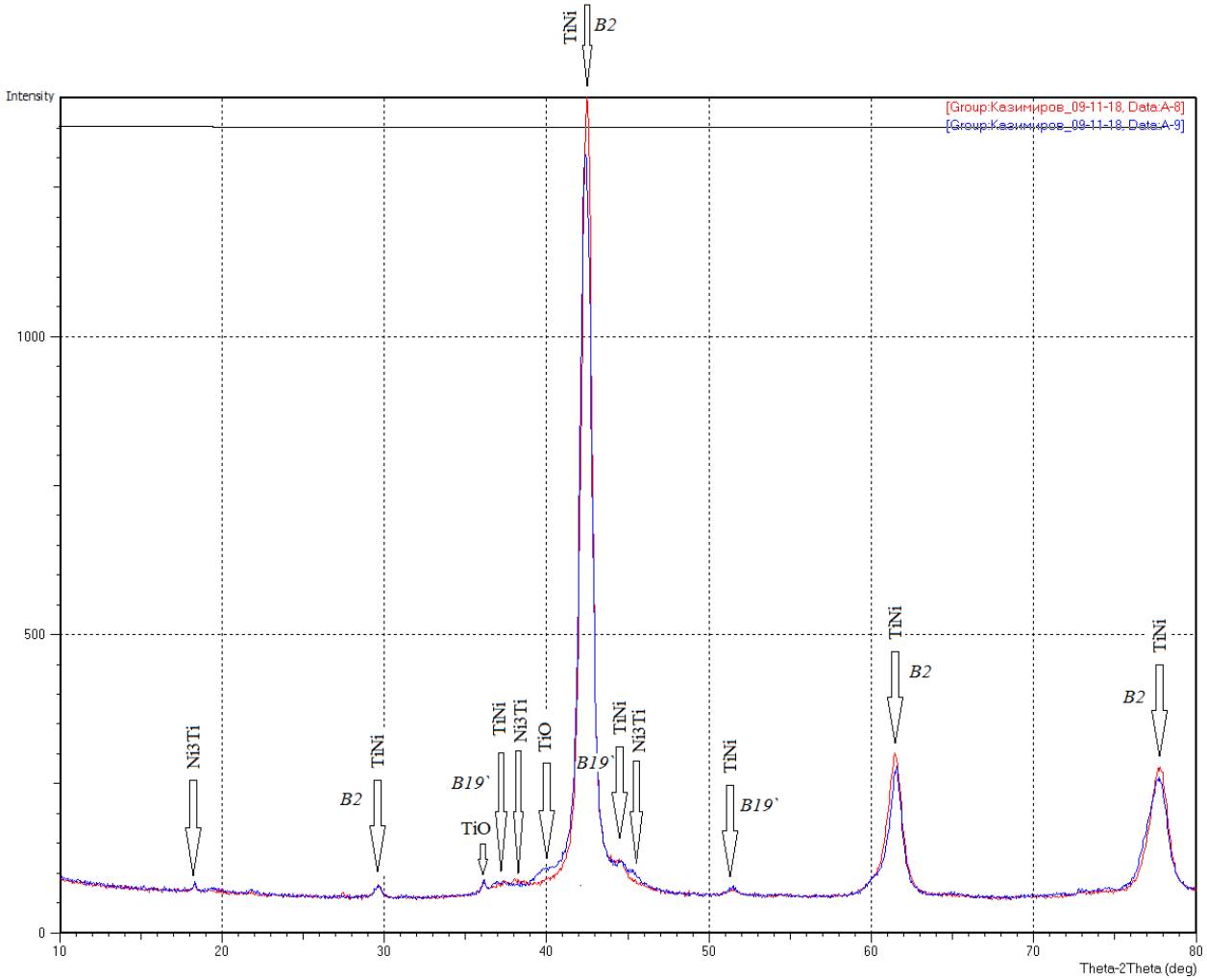

Figure-10. X-ray diagram of the TN-1A alloy phase composition (samples № 8 and 9) after grinding by wheel *i*=2.

Table-3. Volume fraction of phases and intensity in grinded samples TN-1A.

Phase	I, c. u. for dominant peeks*	Relative phase ratio, %			
		Samples		Results	
		8	9	Average	Standard deviation
NiTi B2-phase	2250/1250	75.7	72.8	74.25	2.05
NiTi B19`-phase	250/100	2	8.1	5.05	4.31
Ni3Ti	-/100	4.2	6.9	5.55	1.91
TiO	100/70	18.1	12.2	15.15	4.17

Note: *parent sample/grinded sample

As can be seen from Table-3, the boundary of the B2-phase titanium nickelide content with a cubic lattice is estimated at (74.25 -9.14)% at p=0.95; it was the smallest among all the used wheel characteristics. Titanium oxides with a volume of 15.15% are in second place in terms of intensity. Slightly above the confidence level of 5% there are monoclinic titanium nikelide B19` and secondary intermetallic Ni_3Ti. Because of the alloy strength properties depend on the microstructure and alloy phase composition, it is necessary to characterize the inclusions identified in these diffractograms. As a result of dispersion hardening Ni_3Ti particles enriched with Nickel change the austenitic phase. The coherent phase creates stresses in the matrix, which prevents the movement of phase interfaces during martensite transformations [19]. This phase is characterized as equilibrium one. As a result, the temperature of the end of the MT is shifted to negative temperatures region and the final transformation process is not implemented. TN-1A samples treated by the wheel *i*=2 most likely lost the most in their properties compared to

©2006-2020 Asian Research Publishing Network (ARPN). All rights reserved.

the parent state, although this statement is based on a small volume of the analysis set. Thus, the specified part properties of TN-1A alloy treated by wheel *i*=2 in the above modes can be retained until loading (Figure-2).

According to the X-ray diffraction analysis, TN-1B sample № 2 after grinding with this wheel contains a martensite phase (Figure-11), which was absent in the parent state, and increased fraction of the B2-phase, which is characterized by the intensity of peaks at $2\theta \approx 62^0$, where I increased from 90 to 170 c. u. Unavoidable tensile deformation of the crystal lattice is confirmed by the shift of this peak to the left along the 2θ axis. Titanium oxides are present, but with a fraction relative to the parent state. Among other things, the sample contains a foreign material, the nature of which is not revealed, as evidenced by a narrow peak at $2\theta \approx 18^0$.

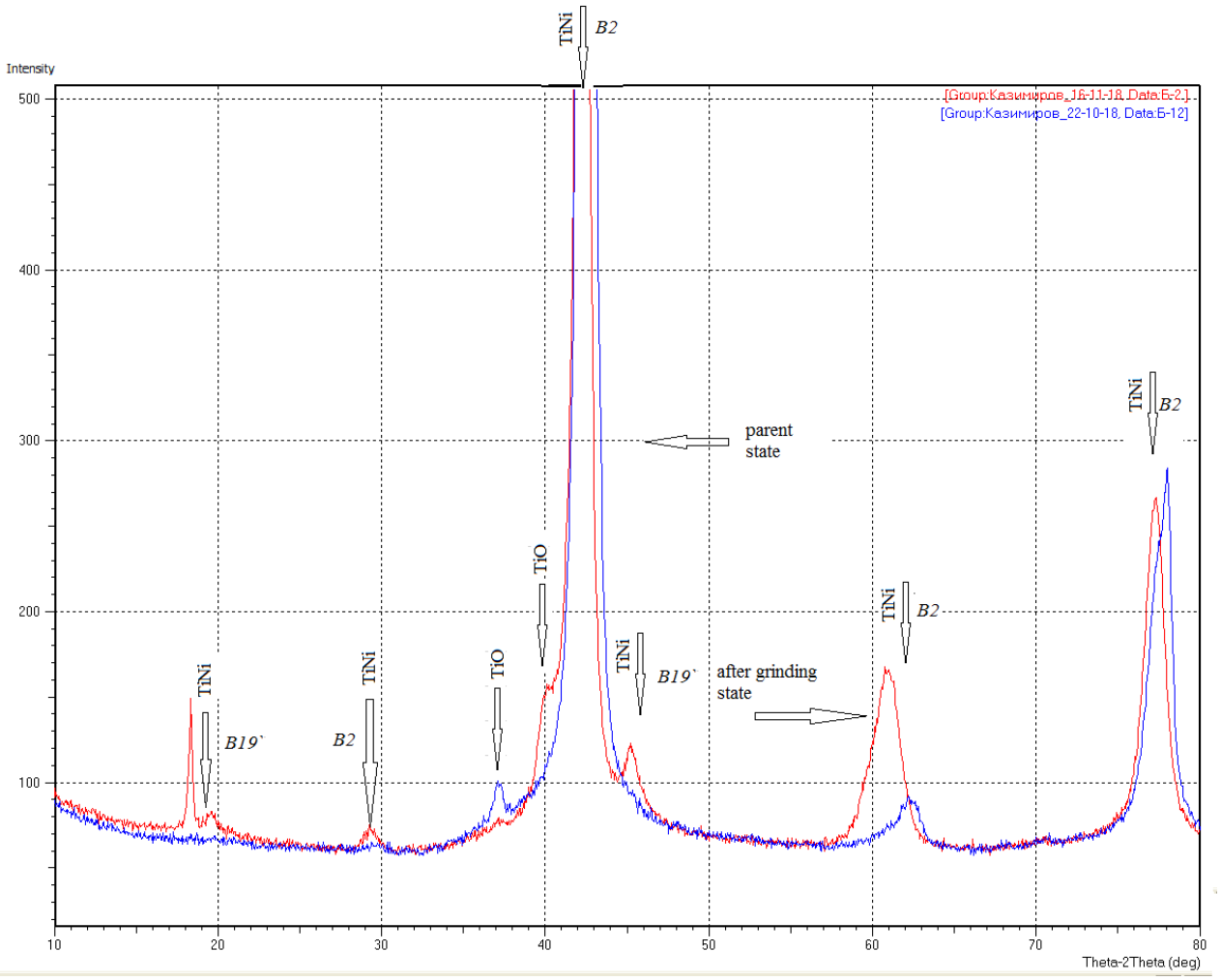

Figure-11. X-ray diagram of the TN-1B alloy phase composition in parent state and after grinding by wheel *i*=2.

Similarly, the analysis of X-ray diffractograms of two samples TN-1B, treated under identical conditions, and compared by phase composition, the results of which are shown in Table-4.

Table-4. Volume fraction of phases and intensity in grinded samples TN-1B.

Phase	Phase fraction, %			
	Samples		Results	
	1	2	Average	Standard deviation
NiTi B2-phase	93.2	83.3	88.25	7.00
NiTi B19`-phase	4.6	4.3	4.45	0.21
TiO	-	9.2	-	-
Ni_2Ti	2.3	-	-	-

©2006-2020 Asian Research Publishing Network (ARPN). All rights reserved.

As can be seen from Table-4, the reliably determined fraction of the solid austenitic phase is 88.25% with a relatively significant arithmetic average, but with high reproducibility error. Average of martensite phase is close to confidence limit. In the samples there is a discrepancy in the diffraction pattern of the secondary compounds. However, this difference may be due to the similarity of the diffraction data in the 2003 PDF-2 database, in particular the dominant peaks, or due to the fact that all Ni-Ti alloys are characterized by selective oxidation of titanium. Note that intermetallic Ni_2Ti is strain-hardened, which is the result of the force action of the tool. It has increased wear resistance [20]. His tracks have been found in sample № 1 (Figure-12). However, in repeated analysis on the sample № 2 for smaller values of the FoM (computed convergence) these tracks are defined as Ti_3O with a large fraction (9.2 instead of 2.3%).

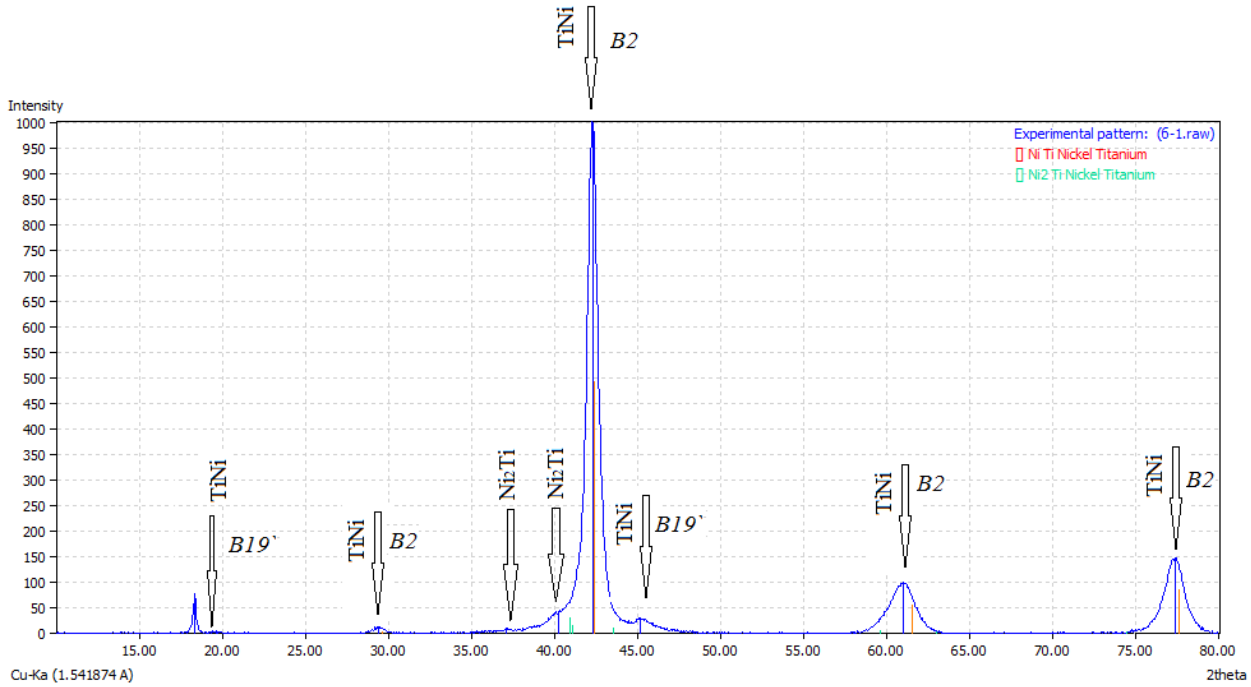

Figure-12. X-ray diagram of the TN-1B alloy phase composition (sample № 1) after grinding by wheel *i*=2.

Grinding by wheel 63C40L7V

Alloy TN-1A, grinded by wheel *i*=3, lost the least in its properties compared to the parent state. Thus, the volume fraction of the austenitic phase with a cubic crystal lattice decreased from I=2250 to 1500 c. u. at $2\theta \approx 43^0$, which is seen in Figure-13 by reducing the intensity of the main peak from I=2250 to 1500 c. u at $2\theta \approx 43^0$. It could be said this decrease was minimal among all previous grinding conditions. Titanium nickelide with a monoclinic lattice partially disintegrated with the formation of a secondary intermetallic Ni_2Ti, which is seen by the peak at $2\theta \approx 45^0$, the intensity of which was I=250 c. u. before grinding. The cubic lattice is less distorted as compared the previous grinding variant and it more meets the reference variant specified in the PDF-2 database.

©2006-2020 Asian Research Publishing Network (ARPN). All rights reserved.

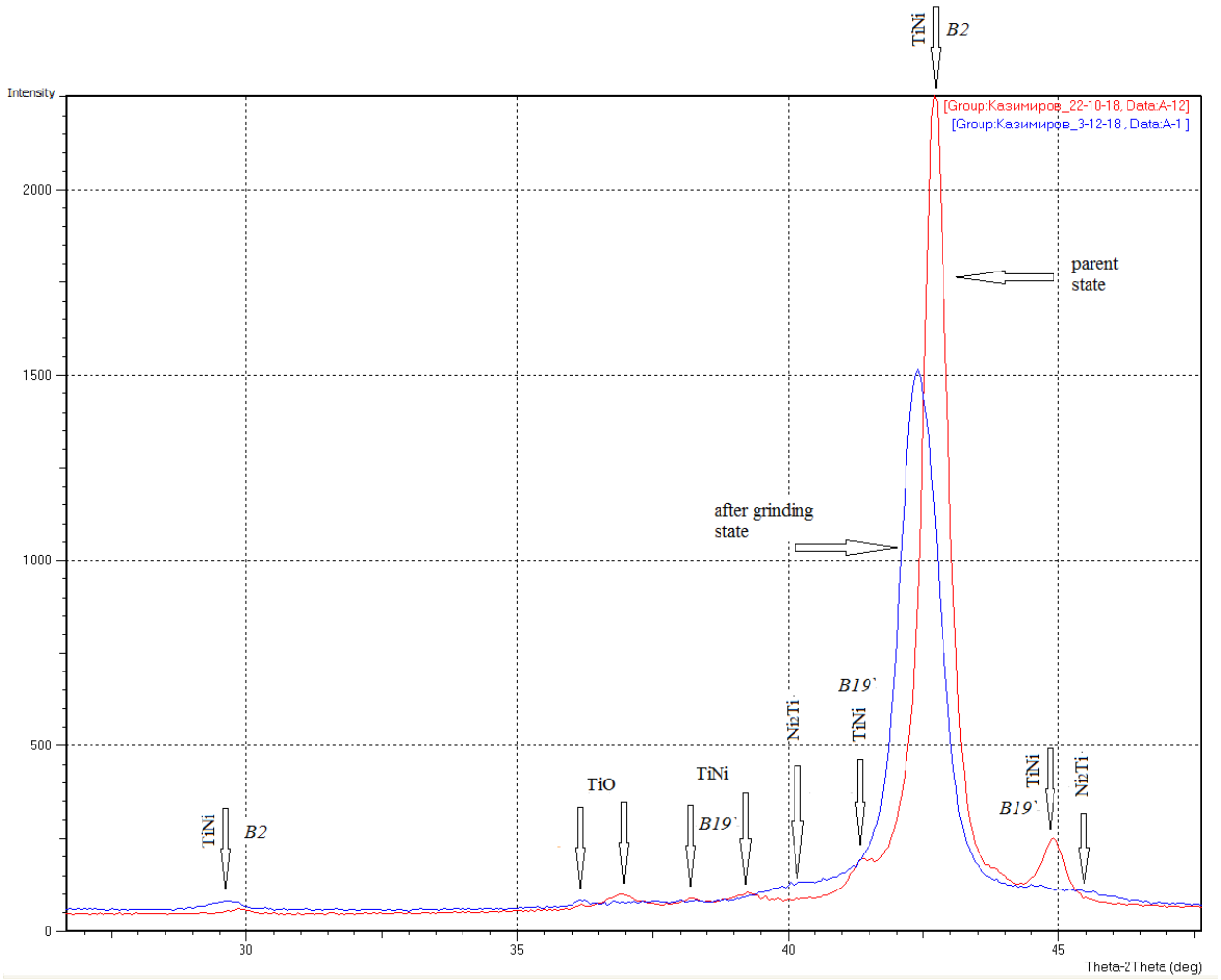

Figure-13. X-ray diagram of the TN-1A alloy phase composition in parent state and after grinding by wheel *i*=3.

It should be note that this is the cheapest of all presented abrasive wheels, but its impact on other quality indicators of the machined surface is not the best of the tools under consideration. Thus, the microhardness estimated on the PMT-3 device at the number of measurements *n*=10 is presented in Table-5.

Table-5. Results of TN-1A alloy microhardness after grinding with different wheels.

Abrasive tool		**Microhardness Hμ, MPa**	
Code	**Wheel characteristics**	**Average**	**Standard deviation**
i=1	08C 070 I12 V01 P1	3348.9	382.9
i=2	08C 046 I12 V01 P1	3349.3	392.6
i=3	63C40L7V	3130.9	529.3

As can be seen, grinding by the wheel *i*=3 led to a relatively lager decrease in the microhardness of titanium nickelide by 370 MPa from the initial value of 3500 MPa, and the stability of the result is predicted to be 1.35 lower than of the compared analogues.

To clarify the reliability of the obtained phase composition, the sample № 2, additionally polished under identical conditions, was subjected to the RiR method of analysis, the result of which is shown in Figure-14 and Table-6.

©2006-2020 Asian Research Publishing Network (ARPN). All rights reserved.

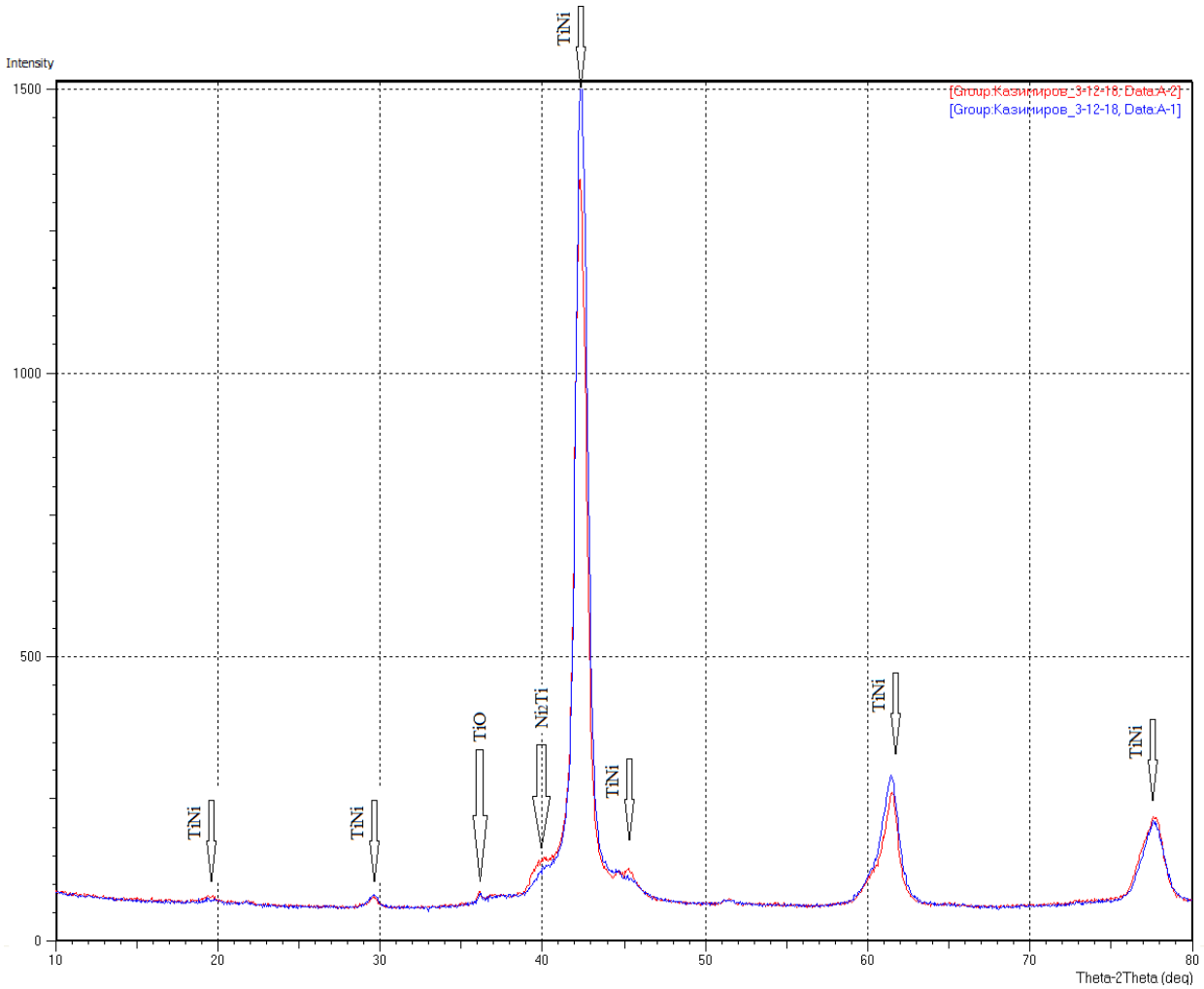

Figure-14. X-ray diagram of the TN-1A alloy phase composition (samples № 1, 2) after grinding by wheel *i*=3.

In addition to the study of phase fraction, intensity of peaks was compared before and after abrasive treatment.

Table-6. Volume fraction of phases in grinded samples TN-1A and comparison peaks' intensity.

Phase	I, c. u. for dominant peaks*	Phase fraction, %			
		Samples		Results	
		1	2	Average	Standard deviation
NiTi B2-phase	2250/1500	91.0	88.9	89.95	1.48
NiTi B19`-phase	250/100	6.7	9.6	8.15	2.05
Ni2Ti	-/100	-	1.5	-	-
TiO	100/-	2.3	-	-	-

Note: * - parent sample/grinded sample

The data in Table-6 show good convergence of results for the austenitic phase. Its lower content limit equal to (89.95-6.62)% is more than after grinding by other wheel characteristics. The analysis showed the smallest of all the variants of the relative content of the remaining phases' fraction. Thus, for NiTi with a monoclinic crystal lattice, the standard deviation is 2.05%, and for the wheel *i*=2 it is twice as high. The presence of secondary intermetallic Ni_2Ti in the alloy is defined as insignificant, and its low-intensity peaks are partially superimposed on traces of titanium oxides. The martensitic phase has a maximum volume content of 8.15% on average. It can be expected that the deformation capability of the grinded samples decreased, and the relaxation capacity deteriorated [21], but to the least extent among those abrasive wheels that were used for the study

©2006-2020 Asian Research Publishing Network (ARPN). All rights reserved.

earlier. The significance of these changes remains to be seen.

The phase pattern after TN-1B alloy grinding by this wheel is similar to the x-ray diffraction analysis obtained for the wheel *i*=2. The phase of austenite B2 also has an increase in peaks' intensity, which will impact on the mechanical properties; similarly, partial degradation in martensitic transformation was observed due to incomplete transformation of B19`-phase.

The difference in two equally grinded samples is observed mainly by titanium nickelide fraction with a cubic crystal lattice and, as a consequence, NiTi with a monoclinic structure. The presence of traces of intermetallics below a reliable 5% level was detected (see Figure-15).

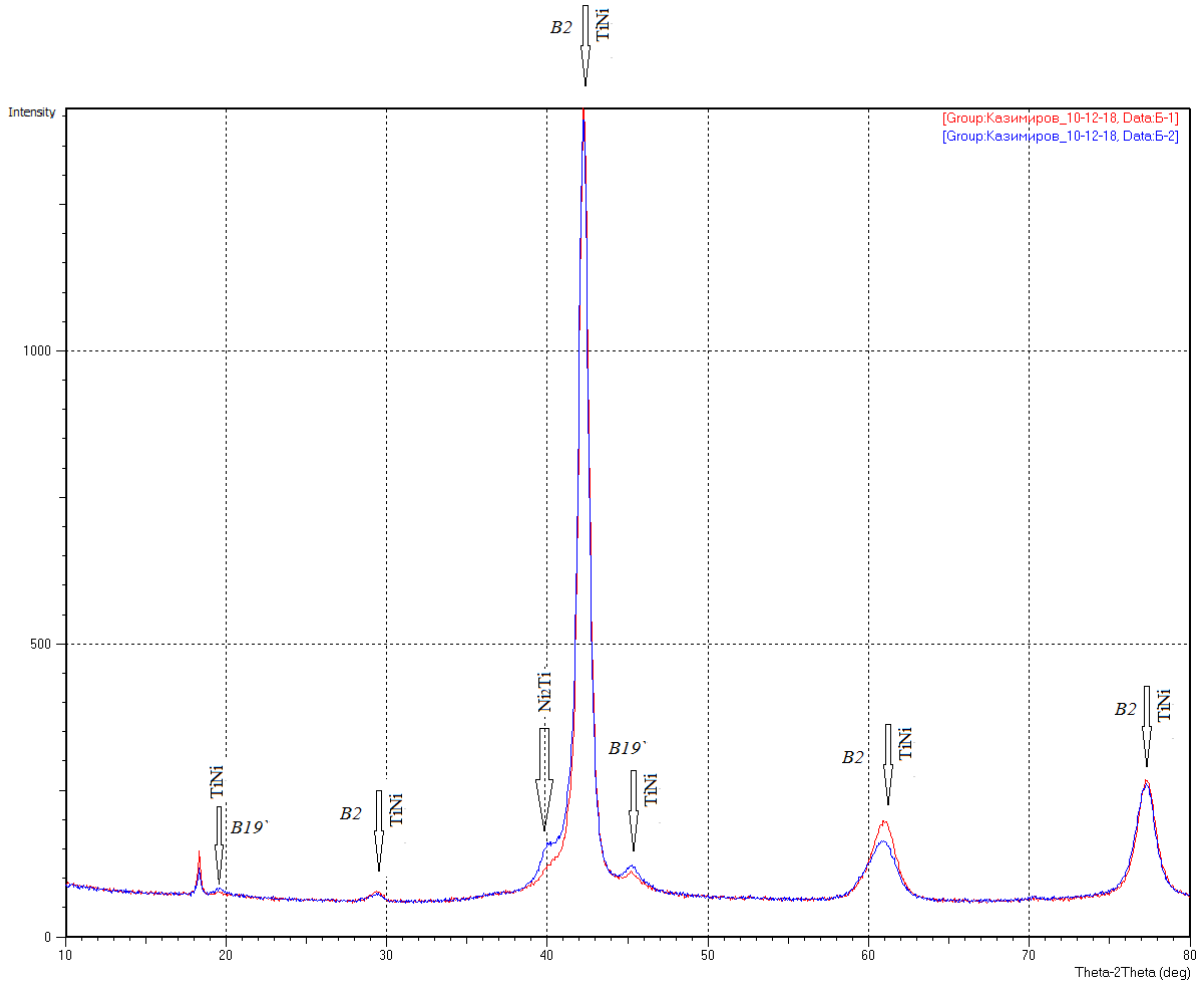

Figure-15. X-ray diagram of the TN-1B alloy phase composition (samples № 1, 2) after grinding by wheel *i*=3.

According to the RiR method, the results on the possible ratio of the studied phases TN-1B that are presented in Table-7 are obtained.

Table-7. Volume fraction of phases in samples TN-1B grinded by wheel *i*=3.

Phase	Phase fraction, %			
	Samples		Results	
	1	2	Average	Standard deviation
NiTi B2-phase	85.1	92.0	88.55	4.88
NiTi B19`-phase	13.6	5.1	9.35	6.01
Ni2Ti	1.3	3.0	2.15	1.20

As can be seen from Table-7, the average volume fraction of the austenitic phase is comparable with the results after grinding with *Molemab* *i*=1, 2 wheels, and this fraction was the smallest by secondary intermetallics.

©2006-2020 Asian Research Publishing Network (ARPN). All rights reserved.

It should be noted that the martensitic phase of titanium nickelide after grinding with this wheel is close to 10%. The peak with the foreign included substance should be excluded from the analysis, as well as in the case in Figure-12.

CONCLUSIONS

Titanium nickeide is quite sensitive to thermal effects and force factor stresses, so when grinding structural-phase transformations occur in the alloy as a result of thermal effects and severe plastic deformation. Grinding tool characteristic has an ambiguous effect on the change in the composition of the stronger B2-phase, the necessary monoclinic structure of the B19`-phase, secondary intermetallic compounds and active titanium oxides. Note that the alloy in the austenitic state at room temperature better retains its diffraction pattern after grinding, and in the martensitic state it is subject to undesirable phase changes. In this case, grinding prevents the restoration of alloy monoclinic structure.

The smallest changes in comparison with the parent state of the nitinol sample with a temperature of Af=351 K were observed after grinding with a wheel of 63C40L7V, which resulted in a decrease in martensitic B19`-phase of the alloy by an average of 9% from the parent 17%.

Grinding of nitinol with reverse MT temperature of 298 K by tool *Molemab* 08 C046 I12V01P1 led to a relatively lower reduction in the austenitic B2-phase, up to 88% compared to the parent state and the irreversibility of 4.5% of martensitic phase content with a monoclinic structure.

However, significant deterioration in the phase parameters were revealed in the alloy TN-1 with reverse MT temperature of 351 K, which was grinded by wheel of this characteristic (*i*=2). This can reduce the performance properties of parts, in particular their strength and reliability.

Grinding of the alloy TN-1 with reverse MT temperature 298 K by wheel Molemab 08 C070 I12V01P1 characteristics is undesirable because it is accompanied by the precipitation of the brittle intermetallic, and the content of the B2 phase decreases to 27% according to statistics. Therefore, the choice of grinding tool characteristics for nitinol requires the creation of special standard documentation, which takes into account the impact on its functional properties.

Acknowledgements this work was supported by Russia Federations №9.6484.2017/8.9.

REFERENCES

[1] Otsuka K. and Wayman C. M. 1998. Shape Memory Materials. Cambridge University Press.

[2] Belyaev S., Prokoshkin S., Razov A., Resnina N., Volkov A. 2017. Preface. Materials Today: Proceedings. Elsevier Ltd. 4(3): 4603-4604.

[3] Blednova Zh. M., Budrevich D. G. 2004. A testing procedure and mechanical properties of materials with the shape memory effect. (Review). Industrial Laboratory (orig. Zavodskaya Laboratoriya. Diagnostika Materialov), Publ. Kluwer Academic/Plenum Publishers. 70(3): 39-46.

[4] Meisner L. L., Markov A. B., Ozur G. E., Rotshtein V. P., Yakovlev E. V., Meisner S. N., Poletika T. M., Girsova S. L., Semin V. O., Mironov Y. P. 2017. Formation of Ti-Ta-based surface alloy on TiNi SMA Substrate from thin films by pulsed electron-beam melting. Journal of Physics: Conference Series, 830(1), [5th International Congress on Energy Fluxes and Radiation Effects 2016, EFRE 2016; Tomsk; Russian Federation; 2 October 2016]

[5] Phillips F. R., Wheeler R. W., Geltmacher A. B., Lagoudas D. C. 2019. Evolution of internal damage during actuation fatigue in shape memory alloys. International Journal of Fatigue. (124): 315-327.

[6] Blednova Z. M., Dmitrenko D. V., Balaev E. U. O. 2018. Tribological properties of multifunctional coatings with Shape Memory Effect in abrasive wear. IOP Conference Series: Materials Science and Engineering, 295(1), [9th International Conference on Tribology, Balkantrib 2017; Cappadocia, Nevsehir; Turkey; 13 September 2017].

[7] Chakraborty R., Datta S., Raza M. S., Saha P. 2019. A comparative study of surface characterization and corrosion performance properties of laser surface modified biomedical grade nitinol. Applied Surface Science. 469: 753-763.

[8] Kaya E., Kaya I. 2019. A review on machining of NiTi shape memory alloys: the process and post process perspective. International Journal of Advanced Manufacturing Technology. 100(5-8): 2045-2087.

[9] Velmurugan C., Senthilkumar V., Dinesh S., Arulkirubakaran D. 2018. Machining of NiTi-shape memory alloys-A review. Machining Science and Technology. 22(3): 355-401.

[10] Miller T., Gupta K., Laubscher R. 2018. An experimental study on mql assisted high speed machining of niti shape memory alloy. Advances in Transdisciplinary Engineering, 8: 80-85, [16th International Conference on Manufacturing Research, ICMR 2018; University of Skovde; Sweden; 11 September 2018].

©2006-2020 Asian Research Publishing Network (ARPN). All rights reserved.

[11] Xi X, Ding W., Fu Y. *et al*. 2018. Grinding of Ti2AlNb intermetallics using silicon carbide and alumina abrasive wheels: Tool surface topology effect on grinding force and ground surface quality. Precision Engineering. 53: 134-145.

[12] Xi X., Yu T., Ding W., *et al.* 2018. Grindability evaluation and tool wear during grinding of Ti2AlNb intermetallics. The International Journal of Advanced Manufacturing Technology. 94: 1441.

[13] Popov M. A. 1981. Grinding Nickel-Titanium Alloys. STIN, #3. Moscow.

[14] Kulkarni V. N., Gaitonde V. N., Hadimani V., Aiholi V. 2018. Analysis of Wire EDM process parameters in machining of NiTi superelastic alloy. Materials Today: Proceedings, 5(9): 19303-19312 [8th International Conference on Materials Processing and Characterization, ICMPC 2018; Hyderabad; India; 16 March 2018].

[15] Lin H. C., Lin K. M., Chen Y. C. 2000. Study on the machining characteristics of TiNi shape memory alloys. Journal of Materials Processing Technology. 105(3): 327-332.

[16] Matlakhova L. A., Pessanha E. M. R., de Carvalho E. A. 2016. Mechanical behavior and structural analysis of a TiNi alloy annealled in the 300 to 500°C range and air cooled. Materials Science Forum. 869: 497-502, [21st Brazilian Conference on Materials Science and Engineering, CBECIMAT 2014; Cuiabá; Brazil; 9 November 2014].

[17] Kotsar M. L., Nikonov V. I., Anyshchuk D. S., Ahtonov S. G., Zavodchikov S. U., Ziganshin A. G., Smirnov V. G., Shtutsa M. G. 2012. Iodide Titanium - Perspective Material for Shape Memory Alloys and Hydrogen-Resistant Alloys for Heat-Exchange Equipment of Nuclear Power Installations. Physics of Radiation Effect and Radiation Materials Science, # 5. Kharkov.

[18] Lotkov A. I., Baturin A. A. 2011. Physical nature of martensite transformations in B2-type Ti compounds and TiNi-based alloys. Physical Mesomechanics, #3. Tomsk.

[19] Martin J. W. 1980. Micromechanisms in particle-hardened alloys Cambridge. New York: Cambridge University Press.

[20] Timkin V. N. 2008. Structural phase state of the diffusion zone and patterns of development of deformation processes in nitrided titanium nickelide . Dissertation for the candidate of technical sciences. Institute of Physics, Strength, and Materials Science SB RAS, Tomsk.

[21] Soldatova M. I., Hodorenko V. N., Gyunter V. E. 2013. Physical-mechanical and strength properties of alloys based on titanium nickelide (TH-10, TH-20, TH-1B). Bulletin of the Tomsk Polytechnic University. No. 2.